

Evaluation of the Air-Demand, Flame Height, and Radiation from low-profile flare tips using ISIS-3D

Joseph D. Smith, Ph.D. and Ahti Suo-Ahttila, Ph.D.,
Alion Science and Technology, Owasso, Oklahoma, USA

Scot Smith and Jay Modi, Zeeco, Inc.
Zeeco Inc. Broken Arrow, Oklahoma, USA

ABSTRACT

Low-profile flare fields pose significant design challenges including elongated flames, adequate air supply to burner tips located on inner rows and high radiation flux from the flame to the surrounding wind fence. Recent work completed by engineers at Alion Science and Technology for Zeeco, Inc. has focused on analyzing the performance of a proprietary burner tip used in large low profile gas flares having upwards of 400 burner tips packed together into a staged piping configuration surrounded by a specially designed wind fence. This paper presents results from the CFD analysis of this gas flare and illustrates the capability of the CFD tool to simulate soot formation, radiant flux, flame shape, and flame height for industrial scale low-profile flare fields. This work was completed in conjunction with flare testing where ethylene was fired through the burner tips. Data collected during these flare tests included video, radiant flux, and sound. Test results were used to calibrate the combustion model and to validate CFD predictions of flame height and air demand. Based on this, predicted flame height and air demand were provided for two full flare field cases. In addition, estimates of radiant flux to the surrounding wind fence were provided.

INTRODUCTION

A series of calculations of flare performance have been made. The purpose of the calculations was to predict air demand under various conditions. In addition, the thermal radiation profile around the flare was also determined. The primary computational fluid dynamics (CFD) tool used in this analysis was ISIS-3D [1, 2, 3]. Previously, ISIS-3D has been used in a variety of pool fire analyses to predict package thermal performance [4]. More recently, ISIS-3D has been applied to flare analysis. In this application, new combustion models have been implemented for handling new fuel mixtures including propane and ethylene. The combustion and radiation models have been compared to flame size, shape, and radiation measurements measured during single-burner and multi-burner tests under no-wind and low-wind ambient conditions.

The CFD model included various details depending upon the case that was run. For a single burner case a computational domain of 6 m x 6 m x 30 m was selected. For a multi-burner case a domain size of 35 m x 35 m x 25 m was selected. For the full field the computational domain was extended 10m beyond the wind fence surrounding the entire flare field.

The main objective of this work was to predict the total air demand and the expected flame height for two operating cases. In addition, the radiation heat flux profile was predicted for the three burner test, and for the full flare field cases.

The three burner simulations were compared to experimental measurements of radiation intensity at ground level located 15 m and 30 m from the burner tip. Results of these measurements provided a partial validation of the overall computational model.

This paper contains descriptions of the various simulations, modeling assumptions and methodology, computational results, and comparisons to experimental data.

COMBUSTION MODEL

The combustion model in ISIS-3D is a hybrid model combining Arrhenius kinetics and turbulent mixing. The kinetics and turbulence models are combined by summing the characteristic time scales. In addition to these dynamic models, sequences of irreversible chemical reactions that describe the combustion chemistry are required. To facilitate an efficient and practical CFD calculation, a minimum number of chemical reactions are used that fulfill the requirements of total energy yield and species consumption and production. From the basis of heat transfer, flame size, and air demand the details of the chemical reactions are not critical so long as the oxygen consumption is correctly balanced for a given fuel type. To this end, both two-step and three-step chemical reaction models for the different fuel types have been used.

A two-step chemical reaction is used for propane. The first reaction considered propane plus oxygen which reacts to produce water, carbon dioxide and soot. The soot yield fraction was assumed to be a constant fraction of fuel consumption and fixed at 2.4% as reported in the SFPE manual [5]. The second reaction consumes soot produced in the first reaction. The two-step reaction approach required a pilot burner at the flare tip to maintain a flame. This requirement was due to the relative size of the computational cells compared to individual jet diameters and the high flow velocities at the tip. Without a pilot flame, the high jet velocities cause the flame to detach and blow out.

For ethylene and mixed gases, a three-step reaction is used similar to the one used by Greiner for JP8 jet fuel fires [6]. In a three-step mechanism, the first reaction burns half the hydrogen contained in the hydrocarbon, and any free hydrogen. The second reaction burns the remaining hydrogen in the hydrocarbons and most of the carbon, with some degree of soot production. The third and final reaction burns the soot produced in the second reaction. This sequence of reactions is more numerically stable since the first reaction has a low activation energy (~20,000 cal/mole) compared to the second reaction, which has a typical hydrocarbon combustion activation energy of 30,000 cal/mole. The low activation energy of the first reaction allows partial combustion at low temperatures, releasing approximately 20% of the hydrocarbon heat of combustion. The partial heat release keeps the fire burning without using a pilot flame. Furthermore, this sequence is closer to that actually found in hydrocarbon fires. Again, the stoichiometric details are not critical so long as the fuel, oxygen, and soot are consumed in the correct proportions.

Propane Combustion model

For propane flames, a two-step chemical reaction is used that burns propane according to the following formula:



The coefficients in the formula are mass weights, not moles.

The Arrhenius kinetics equation and parameters for these reactions were

$$\text{Rate (moles/m}^3\text{/sec)} = X_{\text{C}_2\text{H}_8} * X_{\text{O}_2} * A \text{ Exp}^{(-T_a/T)} \quad (3)$$

Where X is the molar concentration of the species (moles/m³), A is the pre-exponential factor (3.29E10 - 1st reaction and 8.0E11 - 2nd reaction), T_a is the activation temperature (K) (15,922 and 26,500), and T is the local temperature (K).

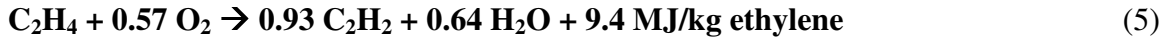
The characteristic time from the kinetics equation was combined with the characteristic turbulence time scale

$$t_{\text{turb}} = C \Delta x^2 / \epsilon_{\text{diff}} \quad (4)$$

Where Δx is the characteristic cell size, C is a user input constant (0.2E-4), ϵ_{diff} is the eddy diffusivity from the turbulence model, and t_{turb} is the turbulence time scale, i.e. characteristic time required to mix the contents of a computational cell. The reaction rates are combined by simple addition of the time scales

Ethylene Combustion Model

For unsaturated hydrocarbon combustion, the requirement of using a pilot flame was eliminated by implementing a three-step chemical reaction. Using this approach, the ethylene combustion model consisted of the following three step mechanism:



As before the coefficients are mass weights, not mole weights.

The Arrhenius kinetics equation and parameters for these reactions were:

$$\text{First Reaction Rate (moles/m}^3\text{/sec)} = X_{\text{C}_2\text{H}_4} * X_{\text{O}_2} * 1.0\text{e}15 \text{ Exp}^{(-10,500/T)} \quad (8)$$

$$\text{Second Reaction Rate (moles/m}^3\text{/sec)} = X_{\text{C}_2\text{H}_2} * X_{\text{O}_2} * 1.0\text{e}11 \text{ Exp}^{(-15,500/T)} \quad (9)$$

$$\text{Third Reaction Rate (kg/m}^3\text{/sec)} = Y_{\text{C}} * Y_{\text{O}_2} * 1.0\text{e}11 \text{ Exp}^{(-20,500/T)} \quad (10)$$

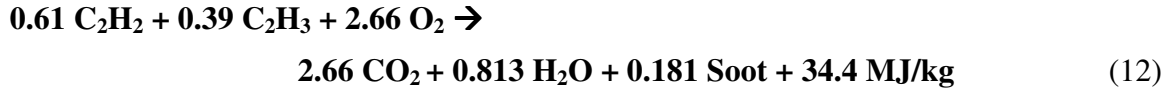
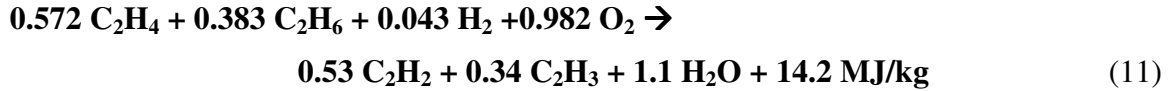
Where X is a mole concentration (mole density) and Y is a mass concentration (partial mass density).

The advantage of the three-step reaction is that the first reaction has a low activation energy, which allows the partial burning and heat release of ethylene. This will maintain combustion since the partial heat released will allow the second reaction, which produces most of the heat and all of the soot, to occur. As in the propane combustion model the ethylene Arrhenius combustion time scale is combined with the turbulence time scale to yield an overall time scale for the reaction rate.

Mixed Gas Combustion Model

A three-step chemical reaction formulation was implemented for a mixed gas having an approximate composition of 32% C₂H₄, 20% C₂H₆, and 34% H₂ (mole percent). Any remaining gases are ignored in the combustion model.

The simplified 3-step reactions are



As before the coefficients are mass weights, not mole weights.

The Arrhenius kinetics equation and parameters for these reactions were

$$\text{First Reaction Rate (moles/m}^3\text{/sec)} = X_{\text{fuel}} * X_{\text{O}_2} * 1\text{e15 Exp}^{(-10500/T)} \quad (14)$$

$$\text{Second Reaction Rate (moles/m}^3\text{/sec)} = X_{\text{mix}} * X_{\text{O}_2} * 1\text{e12 Exp}^{(-15500/T)} \quad (15)$$

$$\text{Third Reaction Rate (kg/m}^3\text{/sec)} = Y_{\text{C}} * Y_{\text{O}_2} * 1\text{e11 Exp}^{(-20500/T)} \quad (16)$$

Flare Nozzle Model

The flare burners have hundreds small holes of various sizes and aligned and divided on each of the eight arms according to the specific tip design. An STL file containing details of the shape and size of the flare arms and supporting structures was imported into ISIS-3D to generate an approximate CAD model of the burner. However the thickness of the arms is on the order of 1 inch, which is below the resolution of the computational grid. As a result the burner model is approximate which is not a problem however because the grid structure has minimal effect upon the fluid dynamics around the outside of the flare burner tip. This minimal flow effect was established by earlier calculations [4] that indicated the primary inflow of oxygen was from the sides of the flare tip and not from below the flare tip.

Point sources of mass, species, and momentum were used to model each hole in each burner. ISIS-3D numerically combines any holes that reside in the same computational cell into a single source. Every hole was included in the simulations so that the mesh structure could be varied without requiring a separate burner file for each mesh structure. Modeling every hole in every burner does cause some additional CPU overhead; however there is less likelihood of an error, since only a single input file is created for all the runs.

To further reduce the likelihood of CAD error that might lead to computational errors, additional FORTRAN programs were used to calculate the flow area, 3-D coordinate location, and direction cosines for each hole in each burner, as well as the mass flow rate and velocity of the flare gas (i.e., propane, ethylene) as a function of driving pressure and temperature.

MODELING ASSUMPTIONS AND APPROACH

The following assumptions were utilized in modeling low profile flares using ISIS-3D:

1. The total air demand for any case was determined by monitoring the flow across a rectangular plane situated at a specified height above the ground, and extending 1-3 meters beyond the edge of the outermost burner. For cases with cross wind, the flow across several planes was monitored and compared.
2. The nozzles were represented as point sources for momentum, mass, and species. The momentum sources included the directional orientation and flow velocity from each hole.
3. The flow velocity exiting each hole was assumed to be proportional to the square root of $\Delta P / (\frac{1}{2} \rho C)$ where ΔP is the pressure drop of the tip, C is a loss coefficient of 0.85, and ρ is the fuel density evaluated at the upstream temperature pressure and molecular weight.
4. For sonic conditions, the previous formula for flow rate which utilized an orifice coefficient of 0.85 and the upstream density and pressure was not used because it is invalid when the flow becomes sonic. Sonic flow is achieved whenever the driving pressure exceeds the pressure where the flow reaches sonic conditions for the specific gas.
5. Combustion of the flare gas was approximated by the appropriate 2 or 3 step irreversible chemical reaction mechanism with specified kinetics.
6. Thermal radiation was calculated using standard radiation models. Radiation shadowing by multiple flares was ignored in the CFD calculation but was accounted for in a separate post-processing calculation that accounted for shadowing and absorption effects.
7. Ambient wind condition, flare gas inlet temperature and pressure, and radiation effects were measured for each test and used in the CFD model.
8. Flame length was estimated from the location where the concentration of intermediate species goes to zero.

ISIS-3D, the CFD tool used for these analyses, is a proprietary computer code for modeling the dynamic behavior of fires influenced by a wide variety of physical processes and is based on the conservation of mass, momentum, and energy. ISIS-3D has been successfully utilized for a wide variety of flow / heat transfer applications [1-4, 5, 6].

The computational domain was extended through the entire flare field. For the full flare field analysis, the wind fence was simulated as a baffle with the appropriate pressure drop to accurately model flow through the fence. The methodology followed to develop and apply the CFD tool to model low profile gas flares included the following steps:

1. Carefully review all flare drawings provided and prepare sketches of the flare tip and the associated flare field. Dimensions not provided were scaled from drawings provided.
2. Set up the geometric domain and generate the computational mesh using the ISIS-3D preprocessor.
3. Select appropriate physical and numerical sub-models (e.g., turbulence, pressure solver, energy, etc.).
4. Perform a single burner simulation to determine the expected flow and temperature profiles around a single burner and compared results to measured experimental data.
5. Perform a three-burner simulation to evaluate burner-burner spacing and compare predicted flame shape/height to measured experimental data.
6. Based on model validation using flare test data, perform a full flare field analysis for a given set of operating and ambient conditions.

Computational Domain

The computational domain used for these analyses (see Figure 1) extended several meters past the edge of all flare tips. For the radiation prediction, the domain extended to a distance of 35 m in both horizontal directions. The height of the domain was normally taken as 15 m except for high pressure cases (20 and 30 psi) where the height was extended to 25 m.

Computational Mesh

Each model utilized different degrees of mesh refinement, with a single burner model having the most refined mesh. A less resolved mesh was used for multi-tip simulations to reduce the overall computational demand required to obtain a converged solution in a reasonable amount of time. As seen, all meshes used were based on rectangular orthogonal cell shapes (as opposed to unstructured cell shapes).

The computational meshes for the single burner, the triple burner, and the full flare field cases are depicted below (see Figure 2). The dense dark to black areas is where the computational mesh is beyond the resolving capability of the graphics. As a result the individual lines congeal into either a dark mass or Moiré patterns (an interference pattern created when two grids are overlaid at an angle, or when they have slightly different mesh sizes). The burner is only depicted in the single burner mesh. In the full field cases the burners could not be fully resolved.

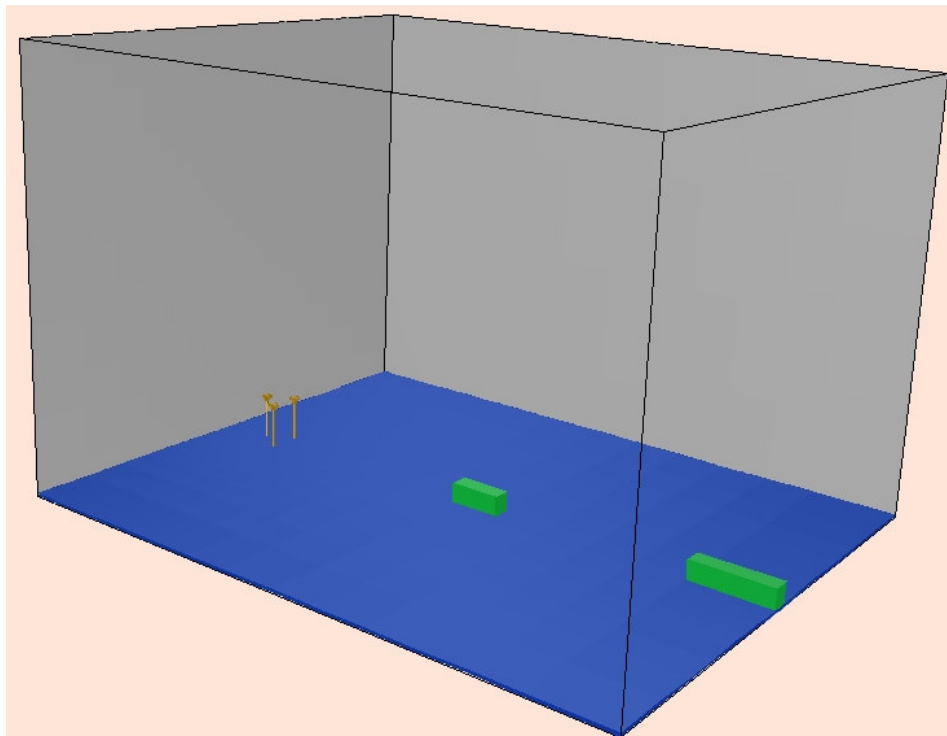
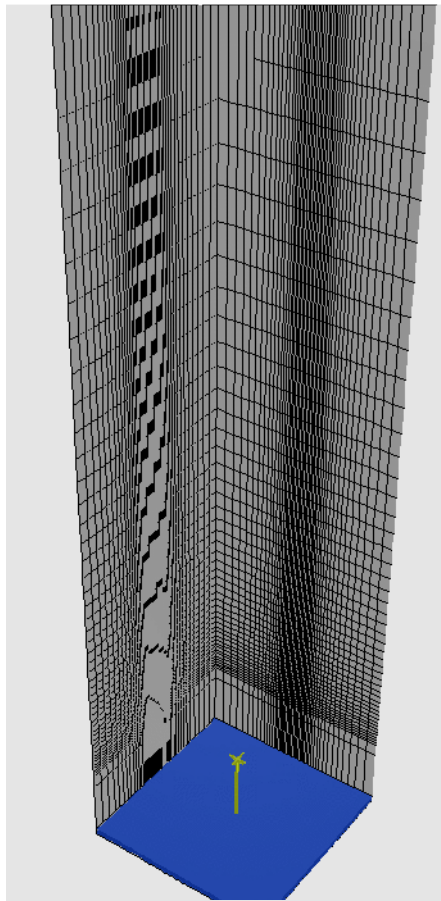


Figure 1 – Triple Burner Computational Domain. The domain size for all analyses was 30 m X 35 m X 25 m. The two green objects shown on the right represent the radiation flux meters located 15 m and 50 m from the flare tip respective

Single Burner Mesh



Three Burner Mesh

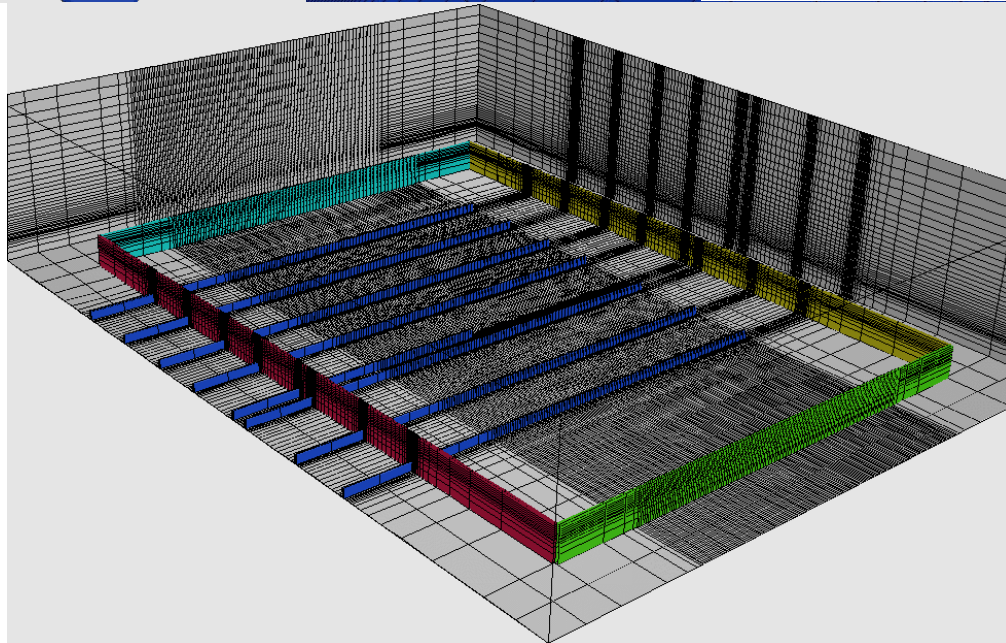
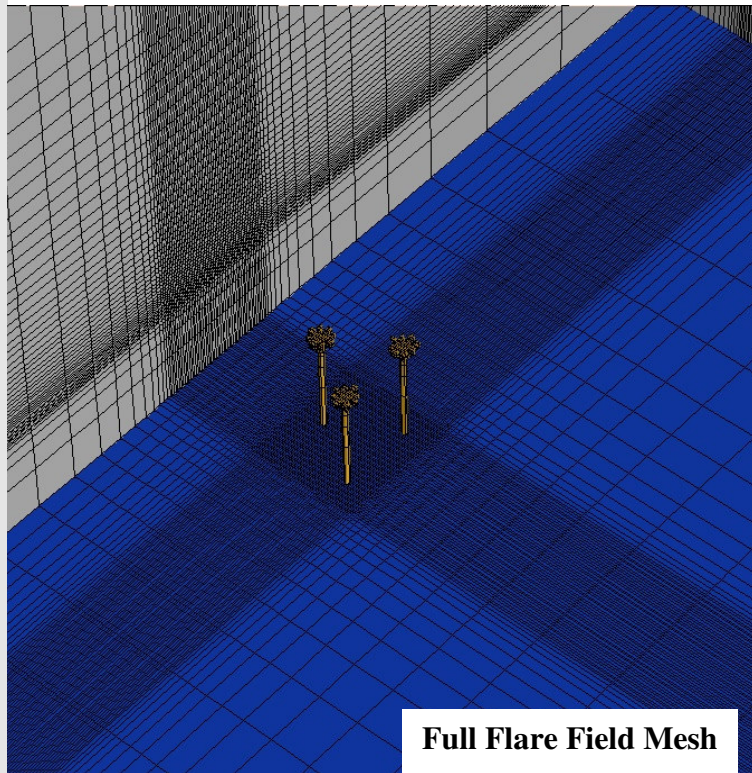


Figure 2– Computational meshes for the single burner case (110,000 cells), the three-burner case (188,000 cells), and the full flare field case (1.2 million cells). Each mesh shows locally fine mesh near the burners

Boundary Conditions

The Boundary conditions used were hydrostatic pressure on all boundaries except the ground. No-flow conditions were selected for the ground surface. The only exception to the hydrostatic boundary condition are those cases where a cross wind was blowing. When a cross wind was simulated, the upstream boundaries were set to the wind velocity and all other boundaries were maintained as hydrostatic pressure conditions.

The thermal and species boundary conditions were set to 300 K (27°C) and air composition respectively.

Physical and Numerical Sub-model Selection

To simulate fluid flow, the momentum solver was the ISIS-3D LES turbulence model. The turbulence plays a role in setting the rate for combustion and mixing of the hot plumes with air.

The energy equation was utilized to capture the temperature changes due to combustion and mixing. The energy equation also included radiation effects.

The species equations were solved to keep track of the distribution and concentration of fuel, oxygen, intermediate species, soot, and products of combustion (CO₂ and H₂O). The combustion model was used to provide the species equations source and sink terms as a function of species concentrations, local gas temperature, and turbulent diffusivity.

ISIS-3D includes a series of models to predict flame emissivity as a function of molecular gas composition, soot volume fraction, flame size, shape and temperature distribution. In turn these variables depend upon solutions to the mass, momentum, energy and species equations. The radiation transport model is used not only to predict radiation flux on external (and internal) surfaces, but it also provides source and sink terms to the energy equation so that flame temperature distribution can be predicted.

Transient Calculation

In each case, the CFD simulation was started with an initial temperature and flow field and run over sufficient time to allow the flow to reach steady (or quasi-steady) state conditions. Steady state was determined by examining flow and thermal variables for relative constancy with time. Since a transient solver was used, all field variables fluctuate in time due to turbulence and other non-linearity's in the equation system. However when examining any field variable, no gradual slope was observed - just short term fluctuations as expected in turbulent flows.

The convergence criteria chosen for the simulations were that the equation of state was always satisfied to within 0.1% or less at any location in the computational domain. Typically the convergence criteria was better than the maximum allowable since the time step constraint was limited by Courant conditions, which allows the flow field to be solved to a higher degree of accuracy.

Post Processing CFD Results

After the calculation converged at steady conditions, appropriate contours of velocity magnitude, temperature, and velocity vectors were prepared. Contours and discussion are presented for each simulation below.

Figure 3 shows a soot isosurface colored by local temperature for a 3-burner test burning propane. Also depicted are grid lines showing mesh refinement near the burners. Also shown is the radiation measuring boxes located 15 m and 30 m from the flare tips. The radiation measuring boxes were objects that were placed into the model from which radiation fluxes could be extracted. These radiation intensity predictions could then be compared to actual measured test data.

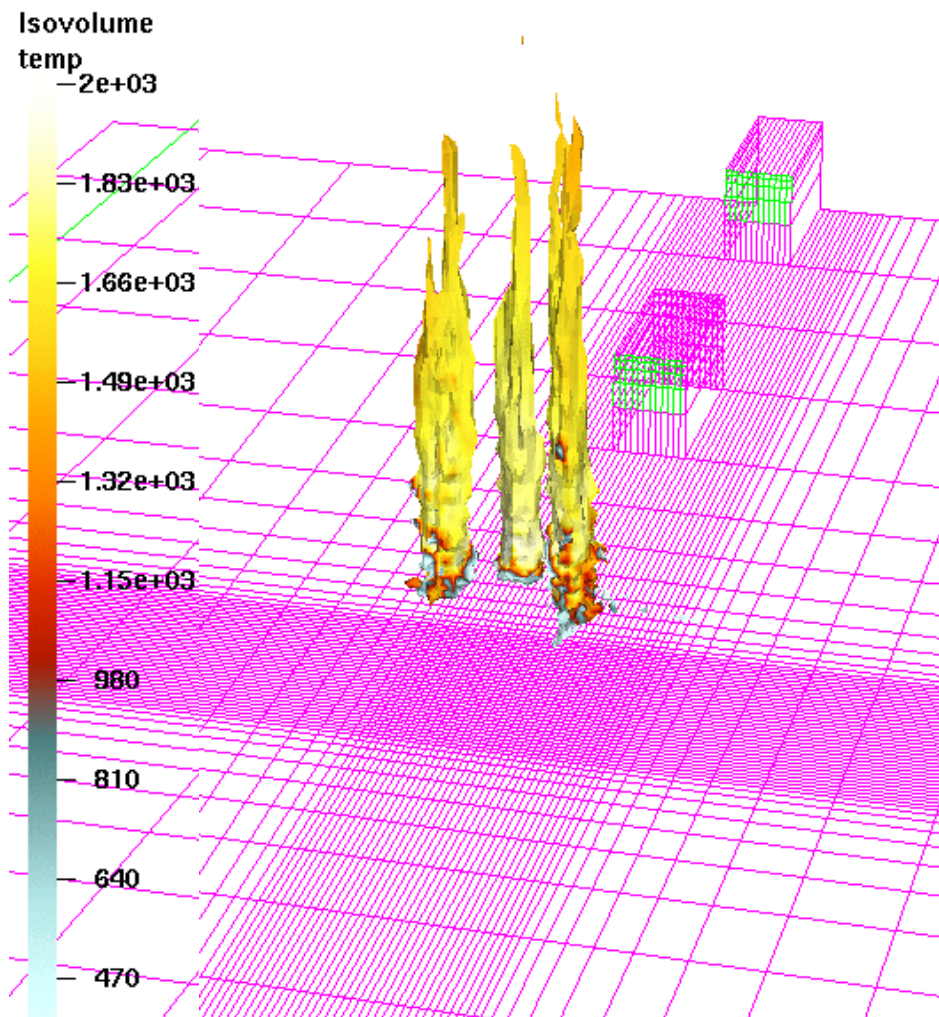


Figure 3 – Soot isosurface colored by temperature in a 3 burner simulation. Also depicted is the mesh and radiation flux monitors

ANALYSES

Single Flare Simulations

Two single flare simulations were performed with two mesh densities. The two flare simulations were of propane and ethylene with the small flare tip. The finer mesh density was used for the detailed simulation for comparison to flare measurements while the coarse mesh was used to test the model under full field conditions. The detailed simulation utilized a mesh density of 97,000 cells (45 x 44 x 49) applied to a physical domain of 6 m X 6 m X 25 m.

By comparing results from the coarse mesh simulation to results from the detailed mesh simulation, the solution was tested for grid dependency and overall accuracy. This provided a method of calibration when applied to the full field simulation. The full field simulation used the same coarse mesh for each burner. Hence, by calibrating the coarse mesh to give the same result as both the detailed mesh simulation and the flare test data, then it can be assumed that the full field calculation is as accurate as possible.

Three Flare simulations

Several three burner flare simulations were performed (see Figure 5 as an example). These 3-burner simulations burned a variety of fuels including propane and ethylene, each at a variety of tip pressures. These simulations were performed on a mesh with 188,000 cells which covered a computational domain of 35 m X 35 m X 30 m so the radiation comparisons to experimental results could be made at distances of 15 meters and 30 meters. The radiation comparisons allowed an evaluation of overall model accuracy.

The radiation intensity depends upon many factors such as combustion chemistry, soot production and burn-up, and fluid dynamics for flame size, shape, temperature and flow velocities. Of all predicted field variables, radiation intensity had the greatest sensitivity to errors and/or inadequacies in the CFD model. Hence comparison to radiation measurements provided the best method of global model validation.

Experimental results for one of the three burner tests are shown in Figure 4. This test was conducted burning propane at the same flow rate used in the three-burner flare simulation shown in Figure 3. The measured flame height for the three burner test was approximately 11.9 meters high compared to the estimated flame height of 12 meters from the simulation.

Full Field Calculations

Four full field calculations were made representing a peak flow case and a sustained mixed gas case without a crosswind. These calculations had a mesh density of over 700,000 cells for the mixed gas case and 1,200,000 for the peak flow case. The physical domain simulated was 10 meters beyond the fence perimeter in all directions with an overall height of 25 m. Results from these cases were used to evaluate the total air demand for the flare as well as the radiation flux to two midpoints on the wind fence.

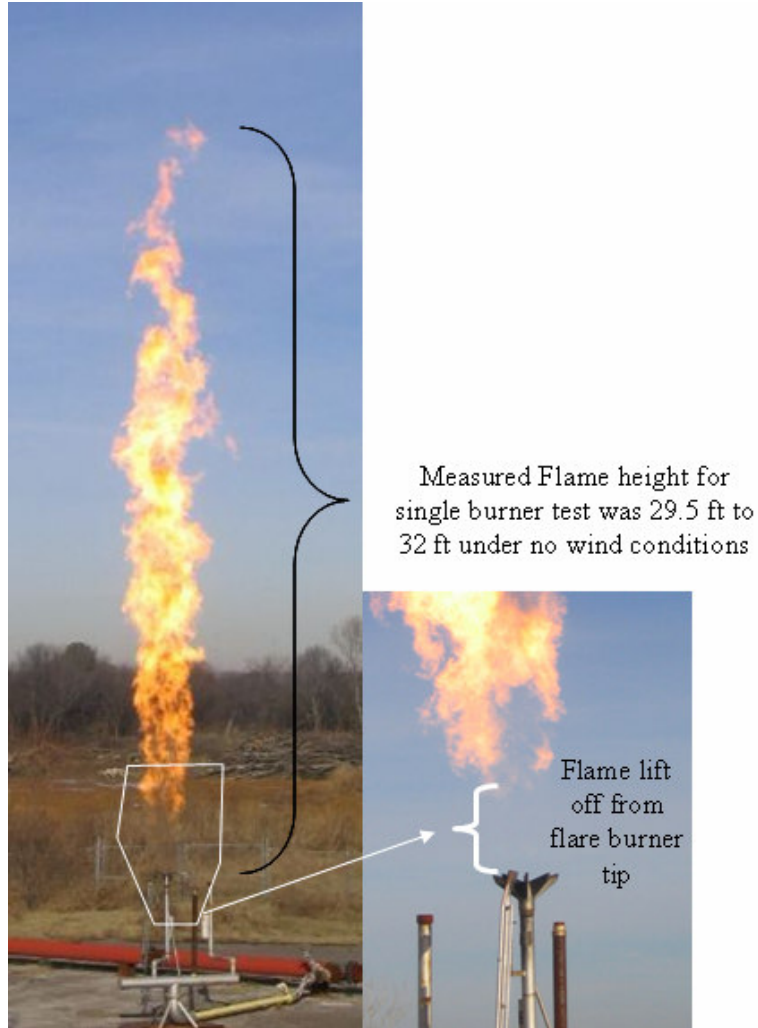


Figure 4 – Experimental measurements of flame shape and flame height for single burner test. Flame lift off represents non-luminous (no-soot) combustion near the tip.

Total Air Demand Results

Total air demand for the full field simulations was evaluated by summing the mass flow crossing a rectangular horizontal plane located at 20 m elevation and vertical rectangular planes surrounding the flare burner (s). This created a box surrounding the flare burner and allowed determination of total air flow. In the absence of a crosswind, flow out through the top plane was sufficient to quantify total air demand, since all other faces had inflow. The total air demand for all of the cases run is presented below (see Table 1).



Figure 5 – Experimental measurements of flame shape, flame height, and radiation flux from a three-burner test firing ethylene under “no-wind” conditions.

Thermal Radiation Estimate

Thermal radiation was estimated for three-burner ethylene flare and the predictions were compared with experiment. Radiation measurements were made for these tests at distances of 15m (50 ft) and 30m (100 ft), three driving pressures (2.8, 7.3, and 11.4 PSIG), and two tip sizes. These radiation measurements allow a comparison of the overall accuracy of the ethylene flare model.

The computational model includes a physical domain of 70 m in horizontal extent by 30 m high. The number of computational cells was 62 X 62 horizontal X 49 high (188356 total). The boundary conditions were hydrostatic pressure on the top surface and as reported constant average wind speeds on the horizontal boundaries. The ethylene was injected at 3 different pressures to represent the experimental conditions. Radiation meters were simulated as vertically aligned surfaces and the incoming radiative flux was monitored on those surfaces.

Table 1 – Predicted Results from Cases Considered. Note all calculations were made for a “no-wind” condition.

Case Description	Evaluation Plane Area (m²)	Total Air Flow (kg/s)	Fuel Flow (kg/s)	Air/Fuel Mass Ratio
Single Burner Propane	14.63	60	0.46	130
1 Burner (Tip 1) Ethylene	13.26	52	0.94	55
3 Burner (Tip 1 - 7.3PSI) Ethylene	36	134	2.88	47
3 Burner (Tip 1 - 11.4PSI) Ethylene	36	144	3.84	38
3 Burner (Tip 2 - 7.3PSI) Ethylene	36	150	4.26	35
3 Burner (Tip 2 - 11.4PSI) Ethylene	36	160	5.79	28
Full Field Peak Flow Ethylene	3226	9700	262.3	37
Full Field Sustained Flow Mixed Gas	1843	4800	93.6	51.3

One complication of the radiation measurement that needs to be included is the effect of the heated ground surrounding the flares and radiation meters. Since the flare is emitting a significant amount of radiation, the ground surrounding the flare heats up. The heated ground emits radiation and that contributes to the overall radiation flux sensed by the meter. In addition to emitting radiation, the ground will also reflect any radiation that is not absorbed. To include the effects of emitted and reflected radiation from the ground surrounding the flares, a ground surface with an emissivity and absorptivity of 1.0 was included in the model. This ground surface was allowed to heat to steady state conditions during the simulation. Using an emissivity and absorptivity of 1.0 allows a reasonable approximation of both emitted and reflected radiation. The overall energy balance for a grey ground surface that both emits and reflects radiation is identical to that which absorbs all the incoming radiant heat and re-radiates it at steady state. Thus a radiation meter, which is assumed to be a grey or black surface, will see the same incoming radiation flux in both scenarios. If the ground reflects radiation spectrally, rather than diffusely then some uncertainty would be introduced into this assumption.

A second effect that was included in the calculations was the atmospheric transmissivity. The atmospheric transmissivity model of Hamins [7] was included for all radiation that passed

through clear air. The Hamins model depends upon ambient temperature, source temperature, and relative humidity. It accounts for radiation absorption by water vapor and carbon dioxide.

Table 2 presents the predictions, measurements, and relative error for 12 different cases.

Table 2 – Radiation Predictions and Test Results Comparison

Tip Size	Position (m)	Burner Pressure (psi)	Total Predicted Radiation (W/m²)	Measured Radiation (W/m²)	Difference (%)
3	15	2.8	2700	3344	-20.0 %
3	15	7.3	4750	4803	-1.0 %
3	15	11.4	6150	6192	-0.7 %
3	30	2.8	650	671	-3.0 %
3	30	7.3	1350	1184	+14.0 %
3	30	11.4	1650	1532	+8.0 %
4	15	2.8	4325	6371	-32.0 %
4	15	7.3	8050	8192	-2.0 %
4	15	11.4	10000	9536	+5.0 %
4	30	2.8	1150	1513	-23.0 %
4	30	7.3	2580	2464	+5.0 %
4	30	11.4	3250	2747	+18.0 %

Note that there were two burner sizes operating at various tip pressures with radiation data taken at both 15 meters and 30 meters. The ISIS-3D predictions are quite good for most of the suite of measurements with the greatest deviations at the lowest pressures. It is not clear what causes the discrepancy between prediction and measurements but the greatest deviations appear to be for the low pressure cases. One potential cause that is not understood may be related to wind effects.

As shown in the table above, when the radiative effects of ground emission and reflection are accounted for, the predicted radiation fluxes are very reasonable, and in some cases quite accurate. The greatest deviation was for the 15 m (50 foot) large tip, where the radiative flux was under predicted by 32%. Otherwise, the predicted fluxes are well within experimental error.

The effect of wind speed upon radiation can be illustrated with the following example. The large nozzle, at a driving pressure of 2.8 psig, was chosen as an example because it had the greatest deviation of all the experimental measurements. The wind speed was varied from zero to 4 m/s (9 mph). The wind direction was 45 degrees toward the radiation meters but not varied in the simulations. Wind causes the flare height to shorten, and may cause flares to merge depending upon wind direction. The calculated radiative flux is shown in Figure 6.

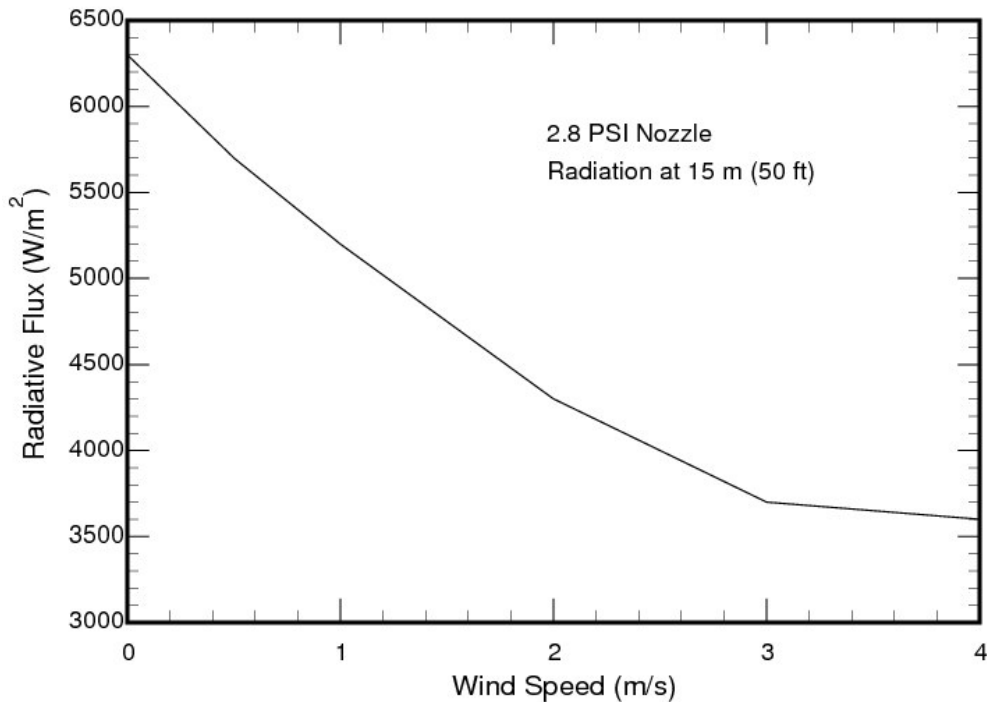


Figure 6 – Effect of wind speed upon radiative heat flux from a triple burner, ethylene flare at a distance of 15 m

The sensitivity of radiative heat flux to wind shown in the figure above illustrates that a momentary reduction in wind speed during the radiation measurement could bring the prediction and measurement into much closer agreement. The experimental data reported a wind speed range, but not the exact speed during the measurement. In the simulations the average of the reported range was used and held fixed during the calculation.

The radiation measurements provide a validation of the overall model because the radiative heat loss from the fire is the single most sensitive parameter to modeling variables. Radiation depends upon flame temperature to the fourth power, flame emissivity, and flame size. All of these variables depend upon solutions to the governing equations, molecular and soot emissivity models, radiation heat transport models, combustion chemistry models, and the overall setup of the CFD model (i.e. Mesh, Wind Boundary Conditions, etc.). If any of the input parameters or models were inappropriate, predicted results would not match experimental measurements as well as shown in Table 2. In conclusion, the good comparisons to test data indicate that the model is validated sufficiently for radiation predictions. This conclusion is based upon the twelve comparisons representing two different nozzles operated at three different pressures each.

The radiation prediction for the full field is more difficult to estimate because radiation leaving one row of burners must pass through other rows before it reaches the fence. When radiation passes through other rows of flares, or portions of rows, some of the radiation is absorbed and re-radiated in other directions. These effects are not considered in the ISIS-3D radiation model. In ISIS-3D, when radiation leaves a flame no checks are made to see if that radiation interacts with intervening objects or other flames. This keeps the code fast running

since shadowing is ignored. When such effects do occur, as in the full field simulation, the user must explicitly account for them in the radiation prediction.

To modify the predicted full field radiation flux to account for intervening flame absorption, a simple numerical model with the following assumptions was made.

1. The flame width and height are equal to the row length and predicted flame height. That is a row of flares behaves as a continuous wall of flames.
2. The flame emissive power is equal to the total radiative heat loss (derived from the ISIS-3D calculation) divided by the radiative surface area (length*width*2) of all the rows.
3. The flux from any row is equal to the emissive power, times the view factor, times an attenuation factor for any intervening rows and the atmosphere.
4. The attenuation factor for any row is equal to $1-e^{-\tau}$, where τ is the optical thickness of the row. The optical thickness of the flames is supplied in the ISIS-3D output.
5. The effect of ground reflection and emission is calculated with the same assumptions and methodology as the 3 burner tests.

A numerical model including these features and assumptions was developed and the results appear in the table below (see Table 3). Radiation intensity at the midpoint of the fences parallel to the burner rows was modeled. Radiation to the midpoint on the fence perpendicular to the rows was not modeled because the rows only partially obscured each other; those cases are labeled (NA). Partial obscuration was beyond the scope of this simple absorption model since it requires significantly more complex view factor calculations.

Table 3 shows predictions for the full field radiation flux to the fences. The radiation predictions directly from ISIS-3D (i.e., not accounting for flare row absorption) are shown in the upper part of the table cell – labeled “ISIS-3D Output”. The radiation prediction modification that accounts for flame absorption due to intervening rows are shown in the lower part of the same cell, labeled (Modification).

Labeling of the walls around the full flare field is taken from a “plan-view” perspective as left-wall, right-wall, and bottom-wall.

Table 3– Predicted Results from Modifications Investigated

WALL	Left Wall	Right Wall	Bottom Wall	Flame
CASE	“ISIS-3D Output”	“ISIS-3D Output”	“ISIS-3D Output”	Optical
	(Modification)	(Modification)	(Modification)	Thickness
	W/m²	W/m²	W/m²	
Case 2	“78,000”	“63,000”	“108,000”	0.275
Peak Flow 944 T/hr	(61,000)	(35,000)	NA	
No Wind				
Case 3	“15,000”	“15,000”	“35,000”	0.28
Sustained 337 T/hr	(6,600)	(6,600)	NA	
No Wind				

Flame Height Estimate

Flame height is difficult to quantitatively assess. The reason is that ISIS-3D predicts flame temperature and species concentrations but does not predict visible light intensity which is what

an observer will rely on to measure flame height (see Figure 4 and Figure 5). The radiation models predict radiation thermal flux, but since the plume above the visible flame contains CO_2 , H_2O , and traces of soot, it still radiates albeit in the infrared. Therefore, an alternate procedure was adopted to predict visible flame height. The procedure selected was to monitor the concentration of ethylene and select the location where the ethylene concentration equals the value corresponding to the measured flame height in the triple burner tests. That ethylene concentration turns out to be a mass fraction of 0.03. Although small amounts of intermediate products and soot may still be present, the driver for all the chemical reactions is the raw fuel. Photographs and measurements of the triple burner ethylene tests reveal that traces of soot do exist in the plume above the visible flame. Thus, monitoring soot concentration overestimates flame height since the soot concentration at the visible limit is not known.

Using ethylene concentration as a predictor of flame height, the peak full field flame heights are shown in Figure 7. The view shown corresponds to a $\frac{1}{4}$ -symmetry no wind conditions simulation. Concentrations shown are iso-surfaces, which are surfaces of constant ethylene concentration equal to a 0.03 mass fraction. The height shown in this image is 25 m. Flames from the leftmost row are approximately 13 m high while flames from the rightmost row are approximately 2 m high. Since Row 1 is a spare, it is not shown. Although only 4 rows are shown, some of the smaller rows have been combined to form a single row to improve computational efficiency.

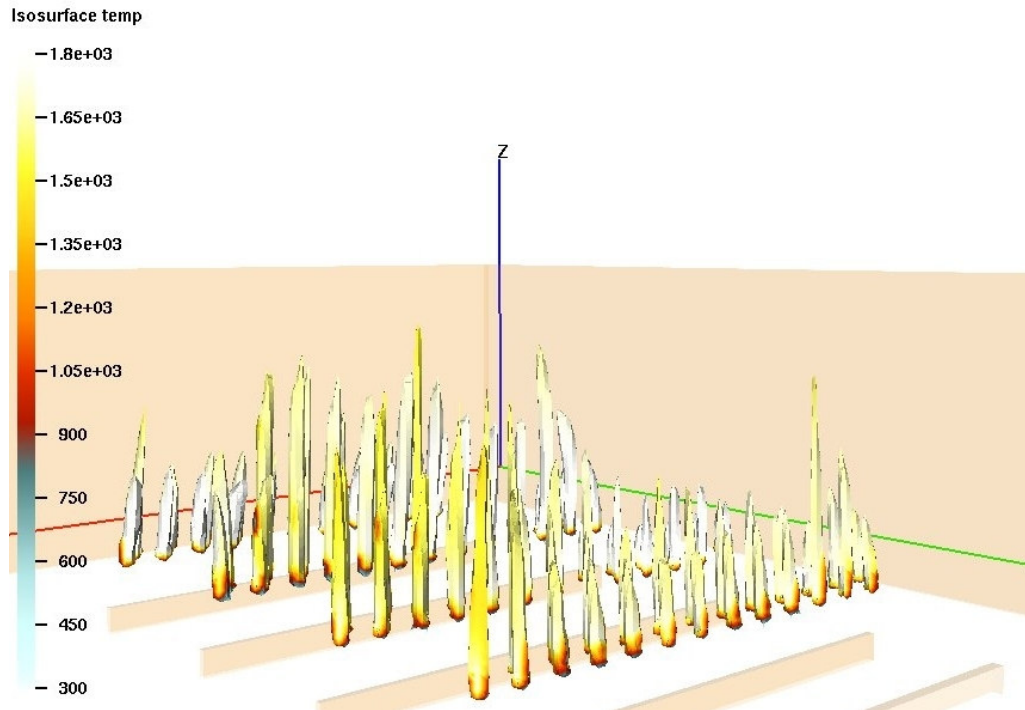


Figure 7 – An isosurface view of ethylene concentration for a $\frac{1}{4}$ symmetry peak flow full field case with no wind. The flame height is shown to be below the fence height.

As shown in Figure 7, the flame height is estimated to be well below the fence level. Although this is a $\frac{1}{4}$ symmetry image, the remainder of the field behaves very similarly. A quarter symmetry problem was chosen to maximize the computational cell density.

RESULTS

The results of these simulations indicate that the total air demand for the various cases is beyond the stoichiometric requirement (stoichiometric requirement varies with fuel type) but is often in the range 15:1 air to fuel mass ratio for many hydrocarbons. The air to fuel ratios for the various cases range from a high of 150 to a low of 38 (using larger flare tip operated at high pressure for the 3 burner test). For the full field analysis, the range was from 40 for the peak flow field to 60 for the sustained case. Thus the calculations results support the conclusion that sufficient air will be entrained and present to burn essentially all fuel for both the sustained and the peak flow cases. One caveat is that these air demand calculations represent the "Total Air Demand" for the system as a whole and do not address the possibility that local air starvation may occur somewhere in the flare field.

The radiation predictions indicated that high radiation fluxes incident on the center point of the wind fence are possible (as high as 100,000 W/m² for peak flow case). For the Peak Flow case, the radiation flux incident on the wind fence ranges from 35,000 W/m² to 108,000 W/m². For the Sustained Flow case the incident radiation to the wind fence ranges from 6,600 W/m² to 35,000 W/m². Flame heights were estimated by monitoring ethylene concentration and selecting the location where the concentration equals the value found for the flame height measurements in the triple burner tests. Iso-surface contours reveal that the flame heights for the peak field with no wind are well below the fence height.

CONCLUSIONS

The work presented in this paper documents a transient flame analysis for the multi-tip low-profile flare. Objectives for this work include predicting the total air demand and the expected flame height for a sustained flow case and a peak flow case burning ethylene. The ISIS-3D CFD model was used to perform the computer simulations for a single burner test and a three burner test to verify model predictions. Based on model verification, the full field was simulated. Full field simulations including all burners in the flare field plus the surrounding fence were conducted. ISIS-3D predictions indicate that sufficient air is entrained through the fence to prevent flame from extending beyond the top of the fence and from generating noticeable smoke for the peak flow case which is considered the limiting case. Radiation fluxes to the wind fence are predicted to be up to 100,000 W/m².

REFERECNES

1. Suo-Anttila, A., Wagner, K.C., and Greiner, M., **2004**, "Analysis of Enclosure Fires Using the Isis-3DTM CFD Engineering Analysis Code," *Proceedings of ICONE12, 12th International Conference on Nuclear Engineering*, Arlington, Virginia USA, April 25-29.
2. Greiner, M., and Suo-Anttila, A., **2004**, "Validation of the ISIS Computer Code for Simulating Large Pool Fires Under a Varsity of Wind Conditions," *ASME J. Pressure Vessel Technology*, Vol. 126, pp. 360-368.
3. Greiner, M., and Suo-Anttila, A., **2003**, "Fast Running Pool Fire Computer Code for Risk Assessment Calculations," presented at the *ASME International Mechanical Engineering Congress and Exhibition*, November 15-21, 2003, Washington, DC.

4. Greiner, M, Are, N., Lopez, C., and Suo-Anttila, A., "Effect of Small Long-Duration Fires on a Spent Nuclear Fuel Transport Package," *Institute of Nuclear Materials Management 45th Annual Meeting*, Orlando, FL, July 18-22, **2004**.
5. Society Fire Protection Engineers, **1995**, *Fire Protection Engineering*, 2nd Edition, National Fire Protection Association Publication.
6. Greiner, M., and Suo-Anttila, A., **2006**, "Radiation Heat Transfer and Reaction Chemistry Models for Risk Assessment Compatible Fire Simulations," *Journal of Fire Protection Engineering*, Vol. 16, pp. 79-103.
7. Fuss S.P., A. Hamins. **2002**, "An estimate of the correction applied to radiant flame measurements due to attenuation by atmospheric CO₂ and H₂O", *Fire Safety Journal*, Vol. 37, pp. 181-190.